Reports on Geodesy and Geoinformatics, 2025, Vol. 120, pp. 101–108

DOI: 10.2478/rgg-2025-0021
Received: 12 September 2025 / Accepted: 9 December 2025
Published online: 23 December 2025

ORIGINAL ARTICLE

The influence of sunlight on the measurement of slender steel pole inclination – A case study

Robert Gradka [1*]

[1]Department of Geodesy and Geoinformatics, Faculty of Geoengineering, Mining and Geology, Wroclaw University of Science and Technology, ul. Na Grobli 15, 50-421 Wrocław, Poland

[*]robert.gradka@pwr.edu.pl

Abstract

Many factors cause the deformation of slender structures, such as the weather conditions that significantly affect their geometry. Surveys of such structures are critical for deformation monitoring and, therefore, general safety. Modern surveying methods like electronic tacheometry (ET), Global Navigation Satellite Systems (GNSS), laser scanning (LiDAR, terrestrial (TLS) and mobile (MLS)), and Unmanned Aerial Vehicles (UAVs) provide means for accurate and effective monitoring. Integrating surveying technologies paves the way for an exhaustive approach to slender structure monitoring and provides accurate data to detect deformation and intervene early. Electricity transmission poles exemplify such structures. The poles need to be monitored regularly to ensure operating stability and safety. The article reports a survey of tubular steel pole deflection angles at various times of the year and under various weather conditions. The surveys were accompanied by temperature measurements and a solar irradiance analysis. The maximum horizontal deflection of the pole top was found to be approximately 27 cm over a single sunny day, highlighting the dynamic nature of solar influence. The analyses yielded conclusions regarding measurements of slender steel structures. Specifically, the study confirmed that solar irradiance can cause short-term deflections of the pole top by up to 27 cm in a single day, and uncertainty increases proportionally with structural dynamics. Consequently, recording precise time and weather conditions during surveys is essential to improve rapid, time-constrained measurement accuracy and the operational safety assessment of slender steel structures. This should improve the measurement accuracy and operational safety of slender steel structures.

Key words: object deflection measurement, tubular power grid pole, sunlight influence

1 Introduction

As societies advance, their requirements for hard infrastructure increase. In the vicinity of settlements, the infrastructure is positioned consistently higher above the ground (Szolomicki and Golasz-Szolomicka, 2019). Reinforced concrete or steel supports become increasingly taller and more numerous. Stacks, cell phone towers, wind farms, and power lines collectively reflect the high demand for such structures. The reliability and good condition of the infrastructure contribute to general safety (Li et al., 2012; Kappes et al., 2012; Feng, 2017; Su, 2020). Infrastructure surveys can identify the geometry of the structures, providing insight into the infrastructure condition (Celebi, 2000; Chen et al., 2001; Roberts et al., 2002; Muszynski and Milczarek, 2017; Roberts et al., 2018; Głowacki, 2022; Tran, 2023; Li et al., 2025). Slender infrastructure assets are affected by several factors detrimental to their condition and operational safety (Chapain and Aly, 2019; Rizzo et al., 2024). Weather conditions, particularly solar heating and wind, are known to produce substantial short-term deformations in slender structures by inducing thermal gradients and dynamic loading. Solar exposure generates non-uniform heating, which leads to temporary bending, while wind primarily contributes to high-frequency lateral oscillations. These combined effects can alter structural inclination to a degree significant for geodetic measurements (Kijewski and Kareem, 2001; Mendis et al., 2007; Breuer et al., 2008; Avini et al., 2019). They can exert long-term impact, be very dynamic (wind gusts), or change cyclically, like solar irradiance. Surveys of slender structures can be rather complicated in a technical and

organisational sense. An extended survey may be subject to errors caused by the displacement of the structure during measurements.

Advances in measurement techniques, such as electronic tacheometry, Global Navigation Satellite Systems (GNSS), terrestrial and mobile laser scanning, LiDAR and Unmanned Aerial Vehicles (UAV) photogrammetry, enable engineers to monitor the geometry of slender structures more effectively and accurately (Lovse et al., 1995; Knecht and Manetti, 2001; Seco et al., 2007; Park et al., 2007; Vezočnik et al., 2009; Sohn et al., 2012; Pandžić et al., 2016; Głowacki et al., 2016; Hauschild et al., 2014; Kwinta et al., 2018; Tran, 2023; Li et al., 2025). Recent developments also indicate a trend towards the integration of measurement data (obtained from terrestrial laser scanning (TLS), InSAR, GNSS, and levelling) and the application of machine learning (ML), which is a subset of artificial intelligence (AI), in geodesy, including the analysis of dynamic deflection data, in order to detect irregularities and anomalies in deformation time series (Nguyen et al., 2018; Li et al., 2022; Liu et al., 2022; Calisi et al., 2023). The solutions and availability of remote measurement methods like LiDAR or photogrammetry – especially on UAVs – streamline measurements and increase the accuracy of geometric representations while reducing costs (Olsen et al., 2010; Wujanz, 2016; Yang et al., 2021; Lu et al., 2022). For instance, Yu et al. (2023) focused on the semantic segmentation of point clouds from LiDAR to recognise pole and wire elements. This step is used for automatic analysis of wire deflection, but above all, it is crucial in preparing data for determining the location of the pole axis. These publications provide arguments for incorporating advanced point cloud processing techniques (UAV, LiDAR, TLS) into the geometry measurement methodology of slender objects. Cross-platform integration improves measurement accuracy and expedites the survey, which is necessary in slender structure displacement and stability monitoring.

The article aims to present the impact of changing weather conditions on the representation of slender structure geometry. The measured and analysed structure is a high-voltage electricity transmission pole (Moschas and Stiros, 2014; Lu et al., 2022; Chen et al., 2023). Such supports are integral to the power transmission infrastructure and must withstand diverse internal and external loads, including wind, ice, mining, and seismic activity (Han and Davidson, 2012; Kwinta and Gawronek, 2016; Komendantova et al., 2016; Luo et al., 2018; Nguyen et al., 2018; Liang et al., 2020). Measurement and monitoring of high-voltage poles are critical for power infrastructure service to ensure the reliability and security of the electricity supply. Precise surveys can detect pole deformation and displacement early, which is essential for preventing failures and optimising power grid service costs (Li et al., 2014; Komendantova et al., 2016; Wang et al., 2017). Such monitoring contributes to the security and reliability of power infrastructure.

To ensure consistency, key references are briefly contextualised throughout the introduction. Instead of listing publications in the first part and describing a single study in detail, in the second part, each referenced work is concisely summarised to highlight its contribution and relevance to slender-structure monitoring.

The article presents the results of surveys of an electricity pole, especially the impact of weather conditions. The research focused on the influence of solar irradiance on the structure geometry. The measurements and analyses facilitated conclusions regarding the methods of surveying slender structures. The novelty of this study lies in the detailed analysis of the dynamic change rate of pole deflection, measured over brief time intervals, in direct correlation with high solar irradiance and vertical temperature gradients. It provides a clearer understanding of the instantaneous errors introduced by solar thermal loading during geodetic surveys.

2 Methods for measuring slender structures

Information about the geometry of slender structures is obtained through surveys. The measurement process can be optimised depending on the structure design and the purpose of the survey. The specific survey method is determined by the shape of the structure and whether it is possible to unambiguously identify or indirectly determine its vertical centreline. Other factors concern the information sought, whether the total inclination, shape, or changes in the shape are investigated. Access to the structure (its visibility) from various points, considering its height, is also important. Optimally, the collimation axis should not be at a vertical angle of over 30 degrees. Much larger angles can certainly be employed (station closer to the structure); however, the accuracy is reduced. Both traditional and new measurement technologies can be used. The conventional surveying methods include:

i. The projection method is the simplest measurement method. It is extremely reliable but offers limited accuracy. It involves projecting points on the structure (selected observation levels) onto a horizontal staff or millimetre scale using a total station. Although measurements may involve multiple stations, two perpendicular directions are typically employed to determine inclination in both planes. Two positions help address a possible instrument error. Results are read directly from the staff (scale), and the distance between the object and the station is also measured. When the scale is positioned at a distance from the structure and instrument, Thales's theorem is employed. The theorem is used to calculate the actual displacement (P) from the measured reading (M) on the scale: $P = M \cdot ld$, where d is the structure-to-instrument distance and l is the structure-to-scale distance, under the assumption that the scale is perpendicular to the line of sight (right angle). The mean inclination error m_p can be calculated with:

$$m_p = \frac{d\sqrt{2}}{l} m_0, \tag{1}$$

where d is the distance between the structure and the instrument, l is the distance between the structure and the horizontal staff and m_0 is the mean error of the mean projection reading.

ii. The trigonometric method involves measuring the structure from several specified and fixed stations (two to six) around the structure, with typically three stations on an equilateral triangle. Horizontal and vertical directions, as well as structure distance, are measured. For this method, the mean inclination error m_p can be calculated with:

$$m_p = \frac{m_k}{\rho} d\sqrt{2} \tag{2}$$

where m_k is the mean error of angular measurements and ρ is a constant (636620^{cc}).

iii. The spatial direction–direction intersection method also involves several stations (at least two) and a total station or theodolite. The stations should be unambiguously fixed and measured, and their positions calculated. The station coordinates and horizontal and vertical directions are used to calculate the coordinates of points on the structure in the adopted coordinate system, with the segments between the stations providing the baseline. For example, the mean inclination error m_p for two stations (in two perpendicular vertical planes) equidistant to the structure can be expressed as:

$$m_p = \frac{m_k}{\rho} \frac{d}{2}. \tag{3}$$

The inclination can also be measured with other methods, such as photogrammetry, laser scanning, or reflectorless rangefinders. Traditional photogrammetry involves taking photographs of the structure from a few stations and calculating the points, as was

the case with the trigonometric method. Today, laser scanning is used, both on the ground and in aerial vehicles. A large number of images can be used to calculate a point cloud with x, y, and z coordinates. The points on the structure can be calculated using distance-distance intersections in space. Today, engineers turn to laser scanning either in its terrestrial form or on UAVs. These surveys yield a coherent point cloud with known x, y, and z coordinates. The structure geometry, such as its centreline or its deformations, can be determined with relative ease.

Modern methods leverage point clouds to assess verticality through analytical approaches such as:

- fitting geometric primitives (e.g., cylinders or cones) to the cloud to define the structure axis;
- employing Principal Component Analysis (PCA) to determine the orientation of the principal axis of the structure;
- generating surface models to quantify deviations from an ideal vertical plane.

Although modern techniques such as TLS or UAV photogrammetry offer superior point density and rapid coverage compared to traditional discrete point measurements, the traditional multi-station tacheometric approach was selected. It provides higher angular precision, direct line-of-sight control to specific observation levels, and full comparability with historical datasets for the same pole. Moreover, the restricted environment around the structure limited the feasibility of deploying scanning instruments at optimal positions.

3 Measurement of a tubular steel pole deflection and inclination

The structure under investigation is a high-voltage, multi-circuit, and dual-voltage tubular steel pole. The pole is made of galvanised structural steel, which is highly susceptible to thermal expansion due to solar radiation. The impact of weather conditions was investigated by measuring a tubular steel pole through spatial distance measurements using electronic tacheometry. The concept of the planned study was to capture the pole centreline position at specific times of the year (summer/winter) and dynamically over a single sunny day (morning, noon, afternoon) to assess the temporal change in deflection caused by solar thermal loading. Three stations (Figure 1) were fixed, measured, and adjusted to obtain their 3D coordinates. The geodetic network adjustment yielded horizontal residuals below 2 mm and vertical residuals below 3 mm, with a global a-posteriori standard deviation of ± 1.2 mm, confirming high internal consistency of the control geometry and ensuring a stable reference frame for the subsequent structural observations.

The control network was measured with a hybrid method (GNSS and direction and distance measurements). GNSS was primarily used to monitor points measured with an electronic tacheometry. Other reasons for using GNSS include faster location retrieval in the field, or the potential reconstruction and staking of points in the field between measurements if they were damaged. Only distance and angle measurements were used to calculate the network adjustment. Standard atmospheric corrections (temperature and pressure) were applied to all distance measurements.

The measurement site is located in an area considered geologically stable, with no history of underground mining or large-scale watercourse influence, thus minimising the risk of long-term foundation displacement affecting short-term deflection results. Prior levelling confirmed that the base benchmarks remained stable throughout the measurement period, with no detectable settlement difference. However, the displacement pattern along the pole height indicates elastic deformations and bending, rather than rigid-body rotation, with upper levels exhibiting disproportionately larger horizontal displacements.

The entire measurement and calculation process was performed

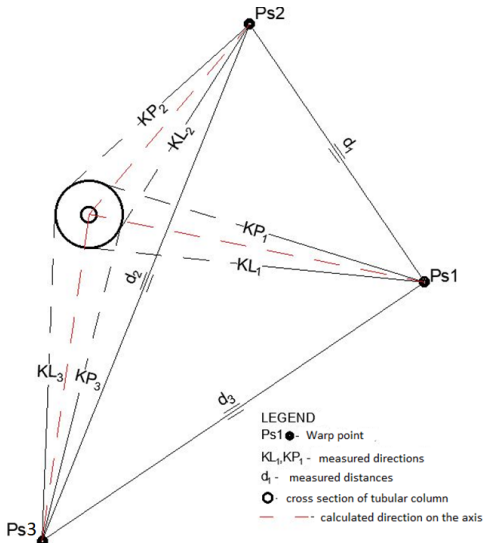

Figure 1. Stations around the structure

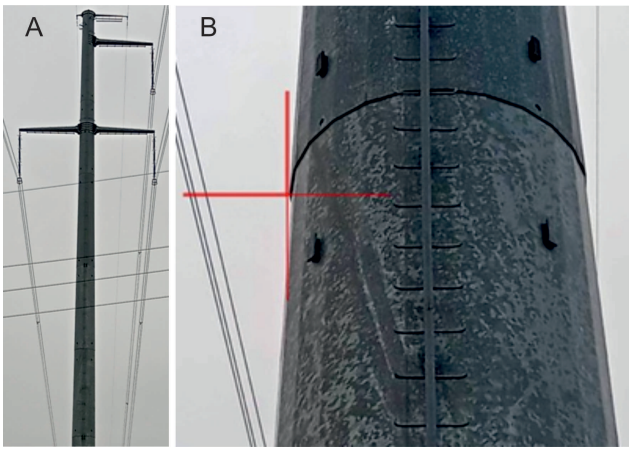

Figure 2. Measured pole: A. View of the pole; B. Crosshairs

in a local coordinate system, which was oriented to approximate the cardinal directions (North, East, South, West) to simplify the analysis of thermal deflection relative to the Sun's path. Specifically, the X-axis was aligned approximately North-South, and the Y-axis was aligned approximately East-West. All results are presented relative to this local, geodetic (North-East) oriented system.

Direct measurement of the centreline of a tubular pole was not feasible because of the presence of buildings on the west and north sides of the pole (Figure 1). It was not possible to establish a measurement point at this location. Therefore, the author measured the tangents to the pole edge and then calculated the centreline – a standard approach to measuring the inclinations of slender structures. Figure 2 below shows the surveyed pole (Figure 2A) with a measured point on the side (Figure 2B). The total pole height is about 63 metres. It is a multi-circuit and dual-voltage system pole. Seven levels were selected for the survey, corresponding primarily to the locations of cross-arms (levels 5, 6) or specific structural joints (levels 0, 1, 2, 3, 4) to capture the pole shape at critical heights.

The first survey session was on July 19th (summer session). The day of the survey was windless, with a nearly cloudless sky and a high air temperature of about +28°C. Before the measurements, the Sun was at an azimuth of 214^{g} and an angular altitude of 62^{g}. At the end of the session, the azimuth increased to 261^{g}, and the altitude fell to 52^{g}. The other survey session was on December 16th (winter session). The day was still and cloudy. The air temperature was about -5°C.

Table 1. Summary of deflection components of the tubular pole centreline in the summer and winter sessions

Level	H [m]	Summer (July 19th) Air Temperature +28°C			Winter (December 16th) Air Temperature -5°C		
		X [m]	Y [m]	m_p [m]	X [m]	Y [m]	m_p [m]
0	7.610	0.000	0.000	0.005	0.000	0.000	0.005
1	15.886	0.016	-0.003	0.004	0.001	0.003	0.004
2	24.466	0.015	0.016	0.004	0.000	0.016	0.005
3	33.197	0.036	0.026	0.004	0.009	0.027	0.004
4	43.319	0.063	0.050	0.004	0.016	0.048	0.004
5	51.806	0.098	0.066	0.004	0.032	0.061	0.004
6	62.844	0.147	0.113	0.004	0.050	0.099	0.005

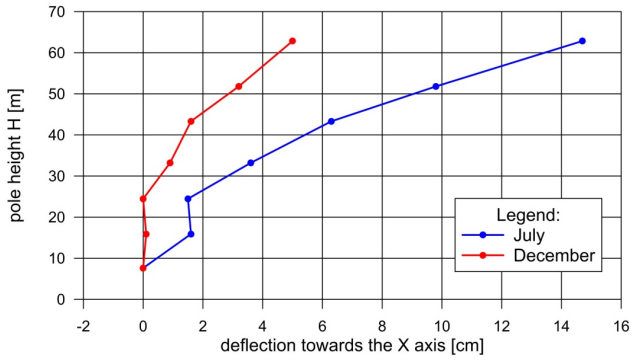

Figure 3. Plot of the tubular pole X-axis deflection component in the H–X plane in July and December

The list of inclination values for two measurements of the tubular pole is presented in Table 1. The inclination values demonstrate that both surveys have similar accuracies on each level of the structure. The pole centreline position errors (m_p) of 4–5 mm are consistent and sufficient for the present analyses, as they are significantly lower than the observed deflections. The high consistency confirms the stability of the control network and the reliability of the measurement procedure over the long-term period. The data in Table 1 clearly show that the deflection component in the X-axis direction (North-South) was significantly larger on the sunny day. This value is approximately three times the winter value. Deflection components towards the Y-axis (East-West) are similar. Figure 3 below shows the X-axis deflection component for various measurement horizons.

Figure 3 shows significantly greater X-axis deflection components in July on every level compared to the December session. In December, the three bottom levels are nearly vertical, and an evident inclination starts from level 3. The inclination values towards

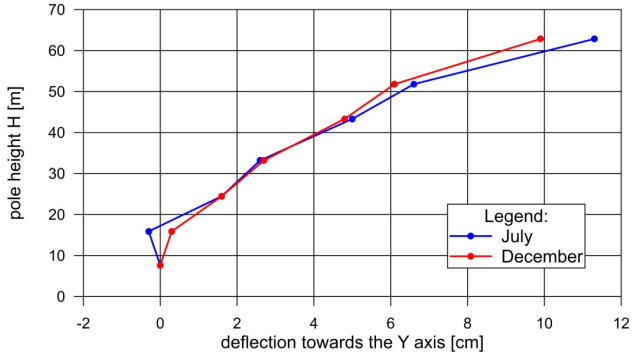

Figure 4. Plot of the tubular pole Y-axis deflection component in the Y–X plane in July and December

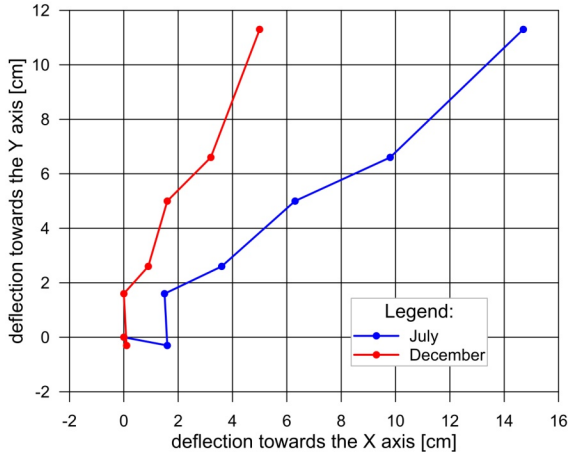

Figure 5. Plot of the tubular pole deflection in the X–Y plane by observation level in July and December

the Y-axis are similar for both sessions, as shown in Figure 4.

The plot (Figure 4) shows that the Y-axis deflection component values are remarkably similar for both sessions on levels 2, 3, 4, and 5. Only level 6 (top of the pole) inclines more on a sunny day. The plot in Figure 5 shows the distribution of centreline inclination in the X–Y plane. The results show that the pole inclined northeast during both sessions, but in winter, it inclined east slightly more (i.e., the Y-axis component was proportionally larger in winter, though the resultant deflection was smaller). The results demonstrate that the pole is inclined Northeast, opposite to the sun-exposed side in July (the Sun was to the Southwest). This suggests that by acting on the pole from the Southwest, the Sun causes it to incline Northeast. Note: The points on the plot (Figure 5) correspond to levels 0 through 6, from the smallest to the largest deflection magnitude.

Considering that the two sessions identified differences between the summer (sunny) and winter (cloudy) measurements, the author decided to conduct a day-long survey session (in March) to investigate the impact of solar irradiance on the structure. In the measurement area, in accordance with the weather forecast and actual conditions, the day was very sunny, windless, and the daily air temperature amplitude was high (21.8°C). The measurements were conducted with a Trimble C5 2" total station (in each measurement in July, December, and March). The temperature was measured with sensor Silicon Labs Si7051 (Board Mount Temperature Sensors ±0.1°C maximum accuracy; human body calibrated digital I2C temperature sensors in 3 × 3 mm; IC: driver/sensor; -40÷125°C) at a height of 1.5 metres above the ground (air temp.) and with the same sensor mounted to the DJI Phantom 4 mini PRO drone at a height of 30 metres and 60 metres. Solar irradiance was measured with Voltcraft PL-110SM. The device specifications include a resolution of 1 W/m^2 (or 1 BTU/(ft^2·h)), a measurement range of 0–1999 W/m^2, and an accuracy of ±10 W/m^2 (or ±5%). All specifications are provided in SI units for clarity. The results are shown in Figs. 6 and 7.

The plot in Figure 6 shows solar irradiance intensity (orange), air temperature (1.5 metres above the ground – light pink), and periods when measurements were taken (light blue). According to the plot, sunrise was at 6:00 a.m. when the air temperature was -4.2°C and solar irradiance was 3 W/m^2. After that, both the temperature and irradiance increased continuously. Irradiance first changed around 8:00 a.m., when it reached 857 W/m^2. The maximum solar irradiance of 1,006 W/m^2 was recorded at 12:30 p.m. The air temperature reached the maximum of +17.6°C at 1:40 p.m. Therefore, the daily temperature amplitude was 21.8°C. The temperature and irradiance declined from 1:40 p.m. till sunset at about 6:00 p.m. A significant variation in temperature and solar irradiance during morning and evening measurements is worth noting.

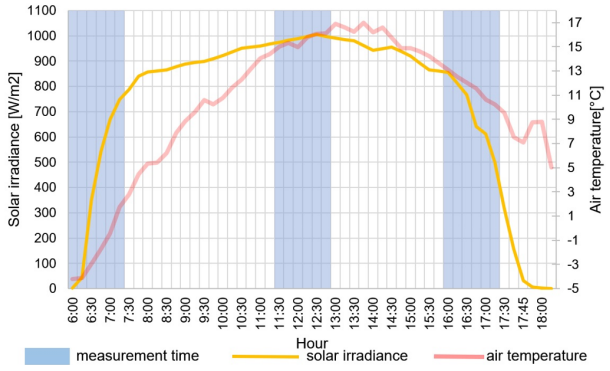

Figure 6. Solar irradiance and temperature on March 13th

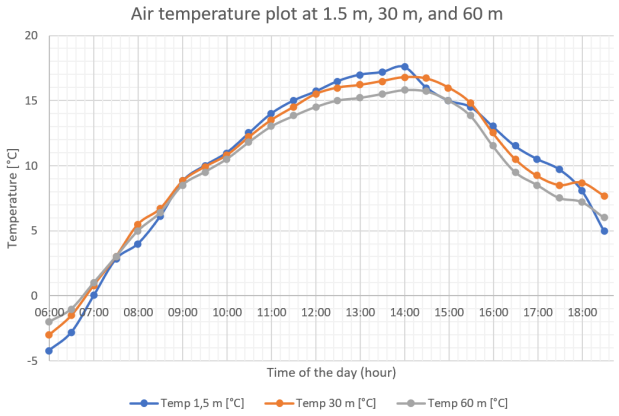

Figure 7. Air temperature plot in March showing profiles at 1.5 m, 30 m, and 60 m

The air temperatures in March, including values measured at 1.5, 30, and 60 metres, are visualised in Figure 7. The temperature at a height of 1.5 m was measured every 15 minutes, while measurements at heights of 30 m and 60 m were taken every 30 minutes. For simplicity, the graph shows measurements every 30 minutes for each height (points).

The plot visually represents a scenario for a sunny day in March, where temperatures generally rise during the day (from min. -4.2°C to max. +17.6°C) and fall towards the evening to +8.1°C. There are slight temperature inversions in the early morning (8:00 a.m.) / late evening (6:00 p.m.) – a higher temperature at higher altitudes than above the ground. Around 6:00 p.m., when heated air near the ground started to convect and the Sun no longer provided sufficient energy to the surface, the author noticed thermal inversion at 30 metres. It was +8.1°C at the ground level and +8.7°C at 30 metres, which means +0.6°C more. Still, at 60 metres, the temperature was +7.2°C. During midday, the temperature is generally consistent or slightly decreasing with altitude due to solar heating and convection.

Figure 8 shows the measured Sun elevation and azimuth on March 13th. The visualisation accounts for the increase in solar irradiance and temperature during the survey. The parameters grow with the Sun's altitude.

The pole H–X inclination plot above (Figure 9) demonstrates that the smallest X-axis deflection component was recorded in the morning. The pole inclined significantly north in the afternoon. The maximum vertical deflection component along the X-axis at that time was 21.4 cm, 11.3 cm more than in the morning. The value declined to 12.0 cm in the evening, which is only 1.9 cm more than in the morning. This plot suggests that solar irradiance leads to a gradual increase in the pole centreline inclination towards the X-axis from sunrise until culmination (meridian transit when the

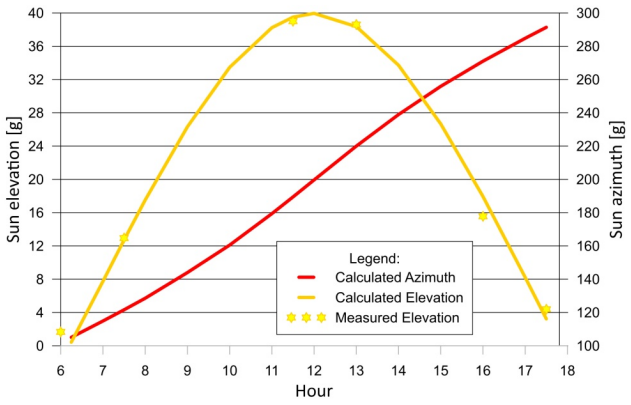

Figure 8. Plot of the Sun's elevation and azimuth on the day of measurement

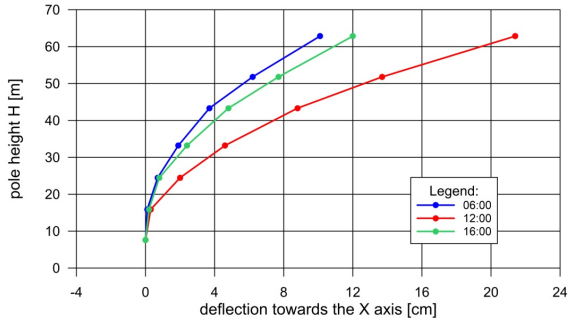

Figure 9. Plot of the tubular pole X-axis deflection component in the H–X plane in March

Sun is at the highest altitude that day). After the Sun reaches the maximum angular altitude and starts the (apparent) descent, the X-axis deflection component begins to return to the initial value.

The plot in Figure 10 shows that the pole plumb towards the Y-axis gradually increases over the day due to solar irradiance and the Sun's apparent movement. In the morning, the top of the pole inclined -3.3 cm west. Then, its eastern inclination increased to reach 7.5 cm at noon and 23.6 cm in the evening. As per the results, the deflection component of the pole top towards the Y-axis varied by 26.9 cm from sunrise to sunset.

Solar irradiance, air and pole structure temperature, and the Sun's position relative to the pole varied over time during the March sessions. The temperature and irradiance analysis shows that the measured weather parameters can vary substantially over 1.5 hours, especially in the morning and evening on a sunny day. During the first session, before the survey, the air temperature was −4.2°C,

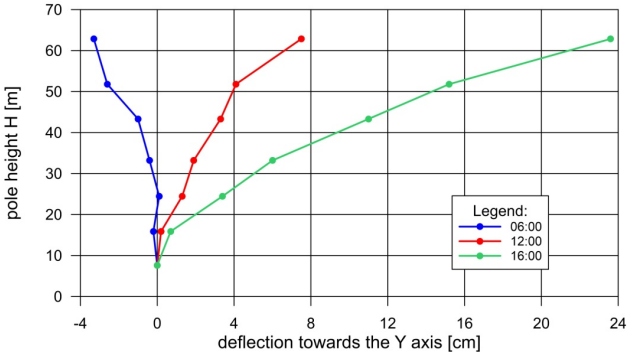

Figure 10. Plot of the tubular pole Y-axis deflection component in the H–Y plane in March

Table 2. Deflection Components and Centreline Position Errors (m_p) at Specific Times on 13 March

Level	H [m]	Winter (December) Air temp. -5°C			Date 13 March Hour 06:00 Air temp. -4.2°C			Date 13 March Hour 12:00 Air temp. +15.5°C			Date 13 March Hour 16:00 Air temp. +12.5°C		
		X [m]	Y [m]	m_p [m]	X [m]	Y [m]	m_p [m]	X [m]	Y [m]	m_p [m]	X [m]	Y [m]	m_p [m]
0	7.610	0.000	0.000	**0.005**	0.000	0.000	0.003	0.000	0.000	0.005	0.000	0.000	0.003
1	15.886	0.001	0.003	**0.004**	0.003	-0.002	0.003	0.002	0.003	0.004	0.004	0.007	0.003
2	24.466	0.000	0.016	**0.005**	0.007	0.001	0.004	0.020	0.013	0.004	0.008	0.034	0.005
3	33.197	0.009	0.027	**0.004**	0.019	-0.004	0.008	0.046	0.019	0.005	0.024	0.060	0.006
4	43.319	0.016	0.048	**0.004**	0.037	-0.010	0.013	0.088	0.033	0.009	0.048	0.110	0.009
5	51.806	0.032	0.061	**0.004**	0.062	-0.026	0.019	0.137	0.041	0.013	0.077	0.152	0.012
6	62.844	0.050	0.099	**0.005**	0.101	**-0.033**	**0.029**	0.214	0.075	0.017	0.120	**0.236**	0.017

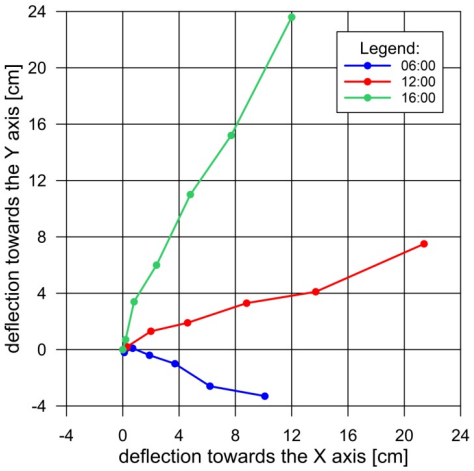

Figure 11. Plot of the tubular pole Deflection in the X–Y plane in March

the structure temperature was -7.9°C, the Sun azimuth was 107^g, and solar irradiance was 3 W/m^2. After the first measurement, the air temperature was +2.8°C, the pole temperature was +4.6°C, the Sun azimuth was 122^g, and the irradiance was 788 W/m^2. It means that the air temperature changed by 7°C, the pole temperature by 12.5°C, the Sun position by 15^g, and solar irradiance by 785 W/m^2 in mere 1.5 hours. The changes in weather conditions were also noticeable during the remaining measurements.

The measurements conducted in December served as a reference point for the stability of atmospheric conditions, as this session was characterized by minimal influence of environmental factors: full cloud cover and a lack of wind, precipitation, and direct sunlight. It was found that dynamic changes in the pole axis position occurred most rapidly in March among the measurement sessions conducted. This was the result of a rapid increase in temperature (amplitude) during the day (from -4.2°C to +17.6°C). Although temperature amplitudes occurring in summer are smaller, the results of the largest deformations during this period are greater than in March (due to the pole surface being heated and heating up during the day). Table 2 below contains the accuracies of adjusted coordinates of the pole centreline on each level (the m_p column).

The first part of Table 2 shows centreline coordinates measured on a windless December day, at significant cloud cover and stable low air temperature of −5°C. The coordinates were adjusted strictly with the constant for each level at 4–5 mm accuracy. It means that precisely the same centreline was aimed at from every station. In contrast, the position of the centreline kept changing between measurements due to the Sun's impact. First, the accuracy of centreline coordinates does not show similar values for every level. Second, it is relatively high and increases with height (as seen in the table - hours 6:00; 12:00; 16:00). The Accuracy of 29 mm does not mean an observer or instrument error. The tangents were acquired correctly from each station, but the pole position was slightly different at every one of them. The charts demonstrate that the inclination grew with the pole height. The highest value was at the top. Therefore, the higher levels can be expected to exhibit the most rapid changes in inclination. This accounts for the centreline coordinate measurement errors growing from bottom to top. This is evidently due to the dynamic parameters affected by the Sun.

4 Summary and conclusions

The literature has amply addressed the issue of weather impact on structure displacement, focusing on steel bridges or reinforced concrete stacks. The surveys presented in this article intend to address several questions that arise when analysing measurement results for power grid poles or, more generally, slender steel structures. Based on the analyses, the following conclusions can be drawn:

i. Air temperature affects geometric deformations of supports. Still, it is less impactful than solar irradiance, the Sun's angular altitude, and azimuth from which it interacts with the structure. The study shows that the angle of incidence of sunrays on the bulk of the pole affects the inclination more than the air temperature. The effect arises from the sun heating the structure, so the structure temperature under the influence of sunlight is a more crucial factor than the air temperature – a phenomenon consistent with established thermal stress models (Breuer et al., 2008). To improve the work, it is necessary to measure the structure temperature directly and simultaneously on the sunny and covered sides at different heights, and to repeat the measurements several times on different days.

ii. The study involved measurements of the temperature of the tubular pole to identify any relationships between its temperature and inclination. Low temperatures of the steel in the structure increase its stiffness, leading to lower inclinations. A high pole temperature increases its plasticity and, consequently, it leads to more substantial geometric deformations – a factor that should be considered in long-term structural health monitoring (Chapain and Aly, 2019).

iii. The tubular pole inclination varies with time of year and time of day. Still, the most significant changes are observed throughout the day, caused by the Sun's apparent motion and changes in incidence angles.

iv. The study further confirms that the inclination of a slender structure depends on its height as well, with higher levels exhibiting more inclination.

v. The measurements of the vertical temperature distribution demonstrated no simple linear relationship with the tubular pole inclination distribution. The tubular pole exhibits consistent directional inclination due to solar load, but the magnitude increases non-linearly with height. At lower levels (0–1), the displacements were sometimes statistically indistinguishable, reflecting the combined influence of structural flexibility and observational noise. The upper levels experience significantly larger displacements, confirming structural bending rather than uni-

form rigid-body rotation.

vi. The inclination of steel structures varies dynamically. Therefore, precise geometry surveys should be completed as fast as possible. Traditional measurements using a single total station on three stations are too slow for the centreline to remain in the same position. This could be mitigated by conducting simultaneous measurements from three stations with three teams, although such an approach is financially straining.

vii. Alternatively, TLS can be employed. Modern scanners can capture the full geometry of a pole within minutes, and a standard two-station TLS survey can typically be completed within approximately 20 minutes. This allows the structure to be considered quasi-static during the scan. While individual point accuracy may differ from precise total stations, the high redundancy of the dense point cloud significantly increases the reliability of axis estimation. Therefore, TLS offers a rapid and effective alternative for monitoring slender structures, minimising the time-consuming constraints of traditional multi-station setups.

viii. It is well established in the surveying community that deflection changes with time of day. However, this study quantifies the rate of change in deflection components (up to 26.9 cm throughout a day) and correlates it with the increasing measurement error (m_p increasing up to 29 mm at the top).

The present results demonstrate that reports of slender steel structure surveys should contain the date and times of measurements, as well as weather conditions and solar irradiance at the times of the measurements. Solar irradiance and the Sun's angular height and azimuth are of particular relevance, too.

Declarations

Funding: No funding was received to assist with the preparation of this manuscript.

References

Avini, R., Kumar, P., and Hughes, S. J. (2019). Wind loading on high-rise buildings and the comfort effects on the occupants. *Sustainable Cities and Society*, 45:378–394, doi:10.1016/j.scs.2018.10.026.

Breuer, P., Chmielewski, T., Górski, P., Konopka, E., and Tarczyński, L. (2008). The Stuttgart TV Tower — displacement of the top caused by the effects of sun and wind. *Engineering Structures*, 30(10):2771–2781, doi:10.1016/j.engstruct.2008.03.008.

Calisi, D., Botta, S., and Cannata, A. (2023). Integrated Surveying, from Laser Scanning to UAV Systems, for Detailed Documentation of Architectural and Archeological Heritage. *Drones*, 7(9):568, doi:10.3390/drones7090568.

Celebi, M. (2000). GPS in dynamic monitoring of long-period structures. *Soil Dynamics and Earthquake Engineering*, 20(5-8):477–483, doi:10.1016/S0267-7261(00)00094-4.

Chapain, S. and Aly, A. M. (2019). Vibration attenuation in high-rise buildings to achieve system-level performance under multiple hazards. *Engineering Structures*, 197:109352, doi:10.1016/j.engstruct.2019.109352.

Chen, L., Chang, J., Xu, J., and Yang, Z. (2023). Automatic Measurement of Inclination Angle of Utility Poles Using 2D Image and 3D Point Cloud. *Applied Sciences*, 13(3):1688, doi:10.3390/app13031688.

Chen, Y., Huang, D., Ding, X., Xu, Y. L., and Ko, J. M. (2001). Measurement of vibrations of tall buildings with GPS: a case study. In *Health Monitoring and Management of Civil Infrastructure Systems*, volume 4337, pages 477–483. SPIE, Bellingham (WA), doi:10.1117/12.435624.

Feng, Z. (2017). *Research on Safety Management and Risk Control of High-rise Buildings*. Theoretical Research in Urban Construction.

Głowacki, T., Grzempowski, P., Sudoł, E., Wajs, J., and Zając, M. (2016). The assessment of the application of terrestrial laser scanning for measuring the geometrics of cooling towers. *Geomatics, Landmanagement and Landscape*, 4:49–57, doi:10.15576/GLL/2016.4.49.

Głowacki, T. (2022). Monitoring the Geometry of Tall Objects in Energy Industry. *Energies*, 15(7):2324, doi:10.3390/en15072324.

Han, Y. and Davidson, R. A. (2012). Probabilistic seismic hazard analysis for spatially distributed infrastructure. *Earthquake Engineering and Structural Dynamics*, 41(15):2141–2158, doi:10.1002/eqe.2179.

Hauschild, W., Lemke, E., et al. (2014). *High-voltage test and measuring techniques*, volume 1. Springer.

Kappes, M. S., Keiler, M., von Elverfeldt, K., and Glade, T. (2012). Challenges of analyzing multi-hazard risk: a review. *Natural Hazards*, 64(2):1925–1958, doi:10.1007/s11069-012-0294-2.

Kijewski, T. and Kareem, A. (2001). Full-scale study of the behavior of tall buildings under winds. In Chase, S. B. and Aktan, A. E., editors, *Health Monitoring and Management of Civil Infrastructure Systems*, volume 4337, page 441–450. SPIE, doi:10.1117/12.435620.

Knecht, A. and Manetti, L. (2001). Using GPS in structural health monitoring. In *Smart Structures and Materials 2001: Sensory Phenomena and Measurement Instrumentation for Smart Structures and Materials*, volume 4328, page 122. SPIE, doi:10.1117/12.435515.

Komendantova, N., Kroos, D., Schweitzer, D., Leroy, C., Andreini, E., Baltasar, B., Boston, T., Keršnik, M., Botbaev, K., Cohen, J., Eismann, C., Hamm, T., Garcia-Aristizabal, A., Keršnik, M., König, M., Kröger, W., Lehmann, M., De Meyer, I., Lemmens, H., and Moeltner, K. (2016). *Protecting electricity networks from natural hazards*. Organization for Security and Cooperation in Europe (OSCE).

Kwinta, A. and Gawronek, P. (2016). Prediction of Linear Objects Deformation Caused by Underground Mining Exploitation. *Procedia Engineering*, 161:150–156, doi:10.1016/j.proeng.2016.08.514.

Kwinta, A., Ważydrąg, K., and Zygmunt, M. (2018). Analysis of power lines span geometry based on TLS measurements. *E3S Web of Conferences*, 55:00013, doi:10.1051/e3sconf/20185500013.

Li, C., Xia, Y., Yang, M., and Wu, X. (2022). Study on TLS Point Cloud Registration Algorithm for Large-Scale Outdoor Weak Geometric Features. *Sensors*, 22(14):5072, doi:10.3390/s22145072.

Li, Q., Shao, Y., Li, L., Li, J., and Hao, H. (2025). Advancements in 3D displacement measurement for civil Structures: A monocular vision approach with moving cameras. *Measurement*, 242:116060, doi:10.1016/j.measurement.2024.116060.

Li, Y., Ahuja, A., and Padgett, J. E. (2012). Review of Methods to Assess, Design for, and Mitigate Multiple Hazards. *Journal of Performance of Constructed Facilities*, 26(1):104–117, doi:10.1061/(asce)cf.1943-5509.0000279.

Li, Y., Du, Y., Shen, X., and Wang, R. (2014). Comparison of several transmission line tower inclination measurement methods. *Hubei Electr. Power*, (38):55–57.

Liang, Q., Liang, S., Peng, J., and Bian, M. (2020). Research on wind resistance and monitoring technology for poleline structure in transmission lines. *Journal of Electric Power Science and Technology*, 35(1):181–186.

Liu, S., Wang, T., Zhang, Y., Zhou, R., Dai, C., Zhang, Y., Lei, H., and Wang, H. (2022). Rethinking of learning-based 3D keypoints detection for large-scale point clouds registration. *International Journal of Applied Earth Observation and Geoinformation*, 112:102944, doi:10.1016/j.jag.2022.102944.

Lovse, J. W., Teskey, W. F., Lachapelle, G., and Cannon, M. E. (1995). Dynamic Deformation Monitoring of Tall Structure Using GPS Technology. *Journal of Surveying Engineering*, 121(1):35–40, doi:10.1061/(asce)0733-9453(1995)121:1(35).

Lu, Z., Gong, H., Jin, Q., Hu, Q., and Wang, S. (2022). A Transmission Tower Tilt State Assessment Approach Based on Dense Point Cloud from UAV-Based LiDAR. *Remote Sensing*, 14(2):408,

doi:10.3390/rs14020408.

Luo, J., Yu, C., Xie, Y., Chen, B., Huang, W., Cheng, S., and Wu, Y. (2018). Review of power system security and stability defense methods under natural disasters. *Power Syst. Prot. Control*, 46:158–170.

Mendis, P., Ngo, T., Haritos, N., Hira, A., Samali, B., and Cheung, J. (2007). Wind Loading on Tall Buildings. *Electronic Journal of Structural Engineering*, (1):41–54, doi:10.56748/ejse.641.

Moschas, F. and Stiros, S. (2014). High accuracy measurement of deflections of an electricity transmission line tower. *Engineering Structures*, 80:418–425, doi:10.1016/j.engstruct.2014.09.007.

Muszynski, Z. and Milczarek, W. (2017). Application of Terrestrial Laser Scanning to Study the Geometry of Slender Objects. *IOP Conference Series: Earth and Environmental Science*, 95:042069, doi:10.1088/1755-1315/95/4/042069.

Nguyen, V. N., Jenssen, R., and Roverso, D. (2018). Automatic autonomous vision-based power line inspection: A review of current status and the potential role of deep learning. *International Journal of Electrical Power and Energy Systems*, 99:107–120, doi:10.1016/j.ijepes.2017.12.016.

Olsen, M. J., Kuester, F., Chang, B. J., and Hutchinson, T. C. (2010). Terrestrial Laser Scanning-Based Structural Damage Assessment. *Journal of Computing in Civil Engineering*, 24(3):264–272, doi:10.1061/(asce)cp.1943-5487.0000028.

Pandžić, J., Pejić, M., Božić, B., and Erić, V. (2016). Tls in determining geometry of a tall structure. In *Engineering geodesy for construction works, industry and research, proceedings of the international symposium on engineering geodesy (SIG 2016), Varaždin, Croatia, 20–22 May 2016*, pages 279–290.

Park, H. S., Sohn, H. G., Kim, I. S., and Park, J. H. (2007). Application of GPS to monitoring of wind-induced responses of high-rise buildings. *The Structural Design of Tall and Special Buildings*, 17(1):117–132, doi:10.1002/tal.335.

Rizzo, F., Caracoglia, L., Maddaloni, G., Sabbà, M. F., and Foti, D. (2024). Exploring multi-hazard effects on a tall building and its non-structural elements through simultaneous earthquake and wind loading. *Journal of Building Engineering*, 91:109489, doi:10.1016/j.jobe.2024.109489.

Roberts, G., Meng, X., Dodson, A., and Cosser, E. (2002). Geodetic signal diagnosis and its applications to structural deformation. In *2nd Symposium on Geodesy for Geotechnical and Structural Engineering, Berlin, Germany, 21–24 May 2002*, pages 111–122.

Roberts, G. W., Tang, X., and Brown, C. J. (2018). Measurement and correlation of displacements on the Severn Suspension Bridge using GPS. *Applied Geomatics*, 11(2):161–176, doi:10.1007/s12518-018-00251-6.

Seco, A., Tirapu, F., Ramírez, F., García, B., and Cabrejas, J. (2007). Assessing building displacement with GPS. *Building and Environment*, 42(1):393–399, doi:10.1016/j.buildenv.2005.07.027.

Sohn, G., Jwa, Y., and Kim, H. B. (2012). Automatic powerline scene classification and reconstruction using airborne LiDAR data. *ISPRS Annals of the Photogrammetry, Remote Sensing and Spatial Information Sciences*, I–3:167–172, doi:10.5194/isprsannals-i-3-167-2012.

Su, Y. (2020). Construction Risk Prevention and Management Countermeasures of High-Rise Buildings in the New Era. *Construction and Design For Project*, pages 224–226.

Szolomicki, J. and Golasz-Szolomicka, H. (2019). Technological Advances and Trends in Modern High-Rise Buildings. *Buildings*, 9(9):193, doi:10.3390/buildings9090193.

Tran, T. S. (2023). Geodetic monitoring of high-rise structures according to satellite determinations. *E3S Web of Conferences*, 392:02041, doi:10.1051/e3sconf/202339202041.

Vezočnik, R., Ambrožič, T., Sterle, O., Bilban, G., Pfeifer, N., and Stopar, B. (2009). Use of Terrestrial Laser Scanning Technology for Long Term High Precision Deformation Monitoring. *Sensors*, 9(12):9873–9895, doi:10.3390/s91209873.

Wang, Y., Han, J., Zhao, Q., and Wang, Y. (2017). The method of power transmission tower inclination detection based on UAV image. *Computer Simulation*, 34(7):426–431.

Wujanz, D. (2016). *Terrestrial laser scanning for geodetic deformation monitoring*. Technische Universitaet Berlin (Germany).

Yang, F., Wen, X., Wang, X., Li, X., and Li, Z. (2021). A Model Study of Building Seismic Damage Information Extraction and Analysis on Ground-Based LiDAR Data. *Advances in Civil Engineering*, 2021(1), doi:10.1155/2021/5542012.

Yu, H., Wang, Z., Zhou, Q., Ma, Y., Wang, Z., Liu, H., Ran, C., Wang, S., Zhou, X., and Zhang, X. (2023). Deep-Learning-Based Semantic Segmentation Approach for Point Clouds of Extra-High-Voltage Transmission Lines. *Remote Sensing*, 15(9):2371, doi:10.3390/rs15092371.